Quantum Electronics **38** (5) 462 – 469 (2008)

LASER RADIATION SCATTERING

PACS numbers: 52.50.Jm
DOI: 10.1070/QE2008v038n05ABEH013741

Properties of laser radiation scattering by a laser-induced spark plasma revisited after 40 years

A.A. Malyutin

Abstract. **Experimental studies of a laser-induced spark produced in air by 1.05-μm, 100-ns pulses with spatial TEM_{00}, TEM_{01} and TEM_{02} modes are described. It is found that when the spark is observed at an angle of 90° to the laser beam axis, the scattered radiation has the maximal intensity outside the beam waist. The intensity ratio of the scattered laser radiation for two orthogonal polarisations is ~ 100, and the spatial structures of their depolarisation considerably differ. These properties are explained by using a model of the Fresnel reflection from the spherical front of the plasma – undisturbed gas interface.**

Keywords: *laser-induced spark, scattering of laser radiation by plasma, depolarisation of laser radiation.*

1. Introduction

After the first publication [1] about the laser-induced spark – a breakdown of gases by focused laser radiation, a great number of papers have been devoted to this object, including some detailed reviews [2 – 4]. It seems that during the period passed after the paper [1], the laser-induced spark, at least initiated by nanosecond laser pulses, should be thoroughly studied. Especially taking into account that at present these studies are mostly applied in character (LIBS – laser-induced breakdown spectroscopy, gas-mixture ignition, high-voltage laser switches, etc.) However, by far not all the phenomena taking place in a nanosecond laser-induced spark (NLIS) have been theoretically explained. In particular, it is still unclear why the transverse size of the plasma channel during the observation of laser radiation scattering by a spark in the lateral direction is only several microns, whereas the laser beam diameter exceeds this value by an order of magnitude or more.

Evolution of a NLIS in gas can be divided into three stages: (i) the gas breakdown in the field of a focused powerful laser beam followed by the formation of a primary plasma in the focal area; (ii) a plasma expansion during the laser pulse when, being within the limits of a caustic of a laser beam, it moves preferentially to the focusing lens; (iii) free plasma spreading out and cooling, the stage which recently [5] has been traced down within 3 ms after the laser pulse termination. For LIBS, the third stage is of most interest because it is assumed to be proceeding under the conditions of local thermodynamic equilibrium [6].

This division into stages concerns NLISs produced by focusing laser beams of diameter D by lenses with the focal distance F satisfying the relation $F/D > 0.05 - 0.1$. Otherwise (especially for multimode laser beams) numerous breakdowns with the total length that can reach several meters [7] are observed in the focal area of a lens, and their spatiotemporal dynamics proves to be rather irregular.

The first stage of the NLIS evolution is sometimes explained by the laser beam self-focusing. However, as shown, for example in [8], nonlinearities of gases under normal conditions are insufficient to lead to self-focusing of radiation. As the most probable processes proceeding during the initial stage of a NLIS, multiphoton ionisation and inverse bremsstrahlung absorption are considered [2, 3, 9]. However, it is not excluded that self-focusing due to enhanced polarisability of excited molecules and atoms of air nevertheless may occur [10].

The second stage – the interaction of laser radiation with a plasma is of most interest from many points of view. It is treated by the majority of researchers as a laser-supported detonation wave (LSDW), which is replenished within the laser beam caustic. During the LSDW propagation to the lens, and in some cases in opposite direction, a long plasma channel is formed. This channel was recorded (integrally during a laser pulse or with the time resolution) at 90° to the beam direction using scattered laser radiation. This scattering, as was shown in many experiments, is actually a reflection on the plasma – nondisturbed gas interface. Thomson or any other kind of scattering are excluded due to the insufficient intensity [11], and also because of strong differences in the plasma images taken from opposite directions [12]. The transverse size of the plasma channel in these measurements limited by the resolution of the optical system was several microns. Anyway, it turned out to be much less than the diameter of the focused laser beam. Interferometric and shadow measurements were also used [13], which gave greater plasma channel diameters than scattering measurements*. Because in this case the plasma channel diameter was also smaller than the laser beam diameter, the effect was attributed to the self-focusing of laser radiation in plasma. It

A.A. Malyutin A.M. Prokhorov General Physics Institute, Russian Academy of Sciences, ul. Vavilova 38, 119991 Moscow, Russia; e-mail: amal@kapella.gpi.ru

Received 10 October 2007; revision received 27 November 2007
Kvantovaya Elektronika **38** (5) 462 – 469 (2008)
Translated by A.A. Malyutin

* Although the detected radiation is reflected from the plasma – undisturbed gas interface, we follow the existing tradition and use the term 'scattering'.

was assumed that the greater plasma nonlinearity can be provided by the polarisability of ionised atoms [14, 15] by the refractive index variation caused by the pressure of light [16]. As an argument in favour of self-focusing, the increased divergence of the laser beam propagated through the focal region was also used [17]. This effect, however, can be also explained by diffraction of laser radiation from the spark plasma [18].

Numerous experiments on the evolution dynamics of a NLIS plasma at the stage of its interaction with laser radiation performed during the period of greatest interest to this object (1964 – 1980) are rather inconsistent. The spatiotemporal structure of radiation of multimode lasers (especially, ruby crystal lasers), which were often used in experiments, was difficult to control. As a result, a NLIS still remains an object for experimental and theoretical studies [19 – 21].

This paper represents the results of experiments that are similar to those performed almost 40 years ago. Careful control of laser beam parameters and the use of the modern measurement technique have allowed us to obtain new and interesting results. We have restricted our studies to observations of scattered laser light by NLISs in air at normal pressure*. The method for detecting this radiation in two polarisations [12] is also used. The experiments are supplemented by modeling the reflection of laser radiation on the plasma – undisturbed gas interface.

2. Experiment

A 1.05-μm single-frequency Nd GLS-23 glass laser emitting Hermite – Gaussian TEM_{00}, TEM_{01} and TEM_{02} modes [22] was used in experiments. The output energy up to 50 mJ was provided by using an amplifier. The laser was Q-switched by using a $LiF:F_2^-$ crystal. The pulse FWHM was 120 ns. The vertical or horizontal polarisation of radiation was produced with the help of two rotatable glass plates mounted at the Brewster angle in the resonator of the master oscillator (denoted by V and H in Fig. 1).

The laser beam was focused by an aspherical lens with a focal distance $F = 8$ mm [23]. The radius of the beam (TEM_{00} mode) measured at the e^{-2} intensity level at the input to the focusing lens $w_{exp} = 1.4 \pm 0.2$ mm corresponded to the calculated beam waist diameter $2w_0 = 3.4 - 4.5$ μm and the Rayleigh length $z_R \sim 12$ μm. The breakdown threshold of air for the TEM_{00} mode in our experiments was 10 – 12 mJ corresponding to the radiation intensity in the lens focus $(1.5 - 2) \times 10^{12}$ W cm^{-2}. To obtain sparks by using higher order laser modes, the radiation energies of the level 15 – 18 mJ were required.

The detection system consisting of a standard microscope objective $10^{\times}/0.22$ and an ELPHEL 313 camera [24] with a CMOS array sensor (3.2 Mpx) was mounted at 90° to the optical axis of the lens (z axis). To obtain simultaneously the spark images in scattered laser radiation for two orthogonal polarisations (v – perpendicular, and h – parallel to the laser beam direction) a birefringent crystal could be inserted between the microscope objective and the camera. Because the laser amplifier introduced some depolarisation to the incident beam, an additional polariser (Glan prism, not shown in Fig. 1) oriented according to the laser radiation polarisation, was mounted in front of the focusing lens.

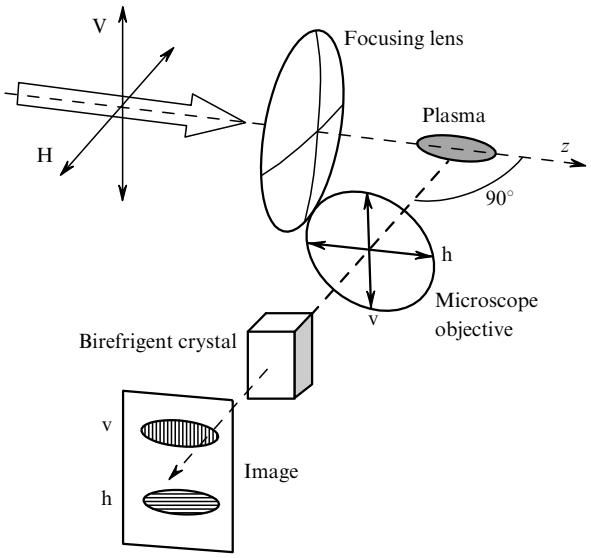

Figure 1. Scheme for detecting laser radiation scattered by the spark plasma.

To measure laser radiation reflected by a spark back into the aperture of the focusing lens, a glass wedge was placed in front of the lens. The beam reflected from the wedge was focused on a LFD-2 photodiode. The laser radiation propagated through the spark was measured by using an objective with the focal distance $F = 50$ mm and NA = 0.95, which also provided the collecting of the main part of the scattered radiation on the photodiode. The detection of the intrinsic radiation of the plasma spark was eliminated by placing IKS-1 filters in front of a CMOS photodetector and photodiodes in all experiments.

Figure 2 shows images of the spark obtained by using TEM_{00} and TEM_{02} laser modes. The image for the TEM_{01} mode is not given because it differs from Fig. 2b only by the angle between sparks ($\sim 29.7°$ for the TEM_{02} mode and $\sim 20.3°$ for the TEM_{01} mode). The modulation of radiation intensity scattered by the spark in Fig. 2c is explained by the presence of two adjacent longitudinal modes with the beat period 5.5 ns. Sometimes near the lens focal plane (beam waist) the intensity modulation could be observed with a small spatial period which decreased with distance from the beam waist. The time resolution of the photodiode was insufficient to measure the beat period in this case.

According to Fig. 2, the transverse size of the scattering region of the plasma channel does not exceed 5 μm. The length of the detected region of scattering changed depending on the excess over the breakdown threshold from $\sim 200 - 250$ μm for the TEM_{00} mode to $\sim 300 - 500$ μm for the TEM_{02} mode. No other specific features in the spark image were observed up to 4 – 5-fold excesses over the breakdown threshold. Laser radiation scattering for the TEM_{00} mode behind the focal plane of the lens is always very weak, while for the TEM_{02} mode it can be detected. In some cases, bendings of the scattering track were observed and the track fracture was sometimes observed behind the focal plane for the TEM_{02} mode (Fig. 2b). In the latter case, two frames made with different attenuating filters in front of

* Although experiments were performed in air without additional cleaning, no spark initiation on dust particles with a low ionisation potential was observed.

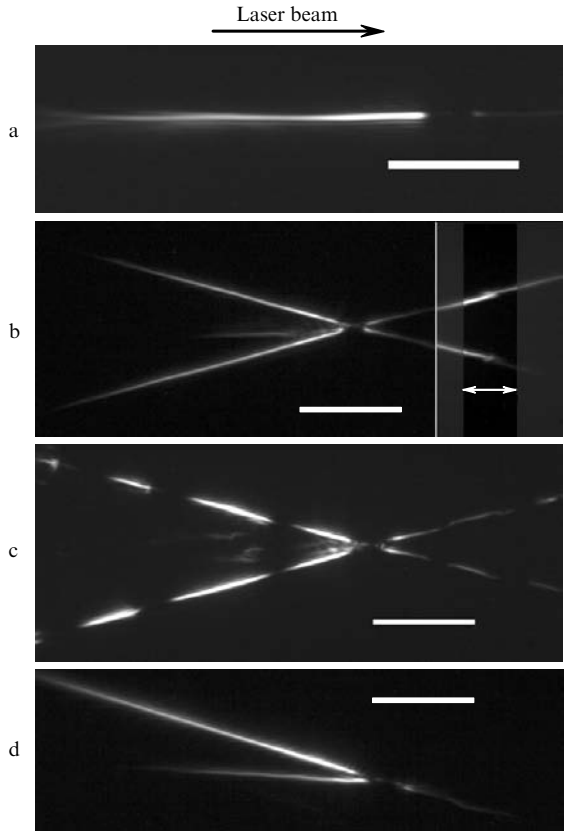

Figure 2. Photographs of sparks in the scattered laser light at their initiation by radiation of the laser TEM_{00} (a), TEM_{02} (b) modes, and the TEM_{02} mode upon intensity modulation with a period of 5.5 ns (c), and by the TEM_{02} mode with one side lobe blocked by a mask (d). Scale 100×5 μm is indicated by white rectangles. The arrows shows the fracture of the scattering track.

the ELPHEL 313 camera were used. In addition, the image contrast in the fracture region (indicated by the arrow in Fig. 2b) was enhanced for better visualisation. The asymmetry of the scattering track intensity for the TEM_{02} mode with respect to the optical axis of the lens in this and other cases is probably caused by poor spatial quality of the initial beam [22].

Note that scattering at the central lobe of the radiation distribution is absent for the TEM_{02} mode. It occurs, however, not because of its lower intensity, which is ~ 0.75 of the intensity of side lobes, but because of turbulence between the upper and lower branches of the track, which is visible in Figs 2b, c. Blocking of one of the side lobes (Fig. 2d) results in an appearance of the plasma channel for the central lobe of the TEM_{02} mode.

All the images of the sparks presented in Fig. 2 were obtained for vertical polarisation of the laser beam (V in Fig.1). Radiation scattered by the spark in polarised light was detected only for the TEM_{00} mode. The results are presented in Fig. 3. The upper parts of Figs 3a, b correspond to the v-component, and bottom parts – to the h-component of scattered laser radiation.

Measurements showed that when vertically-polarised laser radiation was used, the light intensity scattered by the spark was $\sim 80 - 100$ times higher than for the horizontally-polarised beam of the same energy*. Therefore,

* In experiments [12] this ratio was only 2.

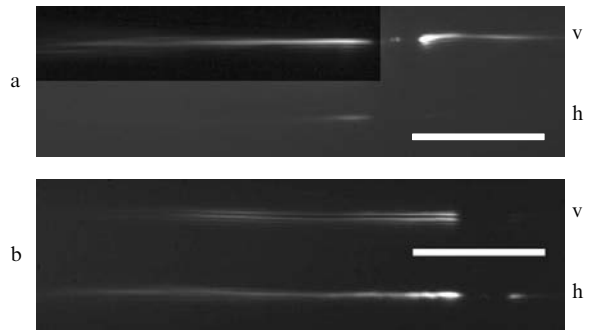

Figure 3. Intensity distributions of the v- and h-components of depolarised scattered radiation (the TEM_{00} mode) for the initial V- (a) and H-polarised (b) laser beams. Scale 100×5 μm is shown by white rectangles.

Fig. 3a corresponding to vertically-polarised laser radiation was compiled of two frames obtained under identical conditions but for differently attenuated radiation.

The structure of images obtained for polarisations of scattered light orthogonal to the initial polarisation is different for V and H polarisations. The images of h-components corresponding to V- and H-polarisations have the identical structure of a single plasma channel. The same structure has the image of the v-component for a vertically-polarised laser beam. However, the image of the v-component for H-polarisation consists of two plasma channels. We will show below that it is caused by depolarisation of the laser radiation on the plasma – undisturbed gas interface at inaccurate orientation of the analyser.

The pulse of the laser radiation (the TEM_{00} mode) reflected back into the aperture of the focusing lens has the leading edge of duration ~ 1 ns and the trailing edge of duration 7 – 10 ns (Fig. 4a). Depending on the laser energy, this pulse could be located either on the trailing edge of the laser pulse (at the breakdown threshold) or on its leading edge (above the threshold) (Fig. 4b). The maximum delay measured between the moment of the spark formation and the laser pulse maximum was ~ 50 ns. According to oscillograms of the radiation transmitted through the spark, the amount of the energy absorbed and scattered by plasma at the breakdown threshold is $\sim 10\,\%$ of the laser pulse energy and increases up to $\sim 45\,\% - 50\,\%$ when the threshold is exceeded by 1.5 – 2 times (Fig. 4c). The absorbed energy was estimated by integrating the area of oscillograms starting from the breakdown onset.

By recording simultaneously oscillograms of the laser pulse and scattering tracks in the presence of laser mode beatings, we measured the dependence of the propagation velocity v of the plasma front on the coordinate z (Fig. 5). Because the resolution of the oscilloscope in the case of high-frequency beatings was insufficient, the parts of the curves adjoining the beam waist (only in this region the scattered intensity modulation had the well resolved spatial structure) first were drawn for the dimensionless velocity, and then were scaled in Fig. 5 to permit the approximation of the dependence $v(z)$ by a smooth curve. Figure 5 shows that the plasma propagation velocity from the focusing lens ($z > 0$) is somewhat lower than in the opposite direction. The beat period indirectly estimated in such a way was 90 – 100 ps.

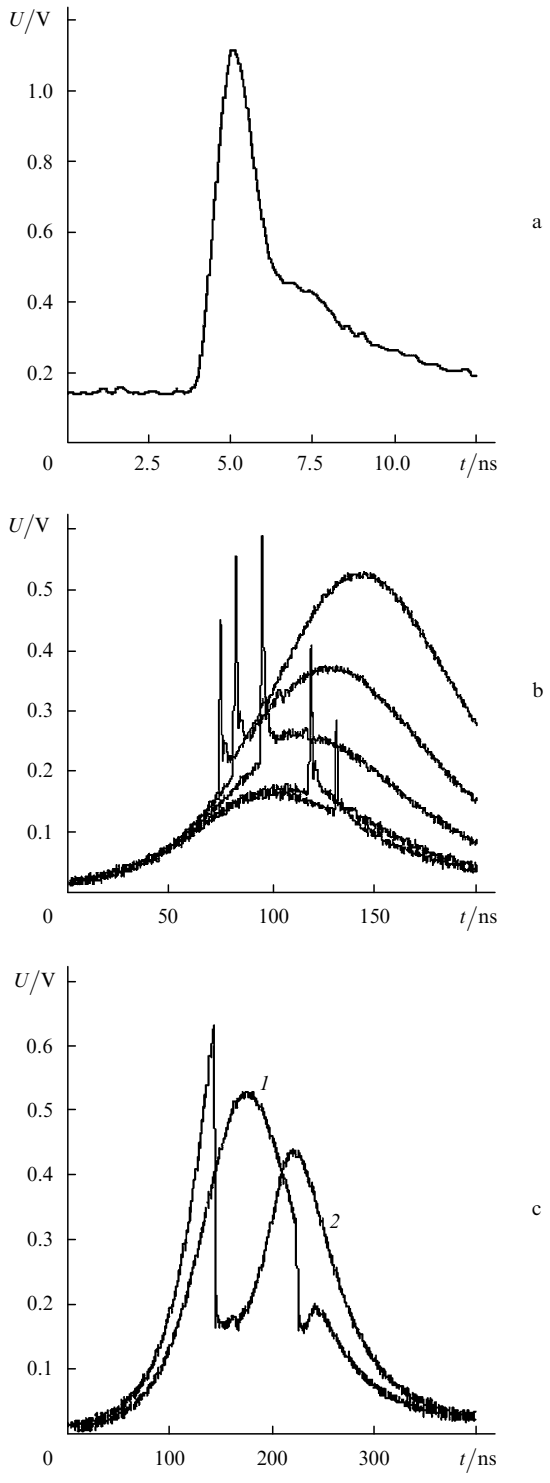

Figure 4. Laser radiation pulse reflected back into the aperture of the focusing lens (a), similar pulses against the background laser pulse scattered by the lens surface (lower trace corresponds to the breakdown threshold) (b), and laser radiation pulses propagated through the spark at the breakdown threshold (*1*) and at the level 1.5–2 times above the threshold (*2*) (c).

3. Discussion

It follows from experimental results that

(1) in the beam waist [$\pm(20-25)$ μm from the focal plane of the lens] scattering of laser radiation is very weak although the laser radiation intensity here is maximal;

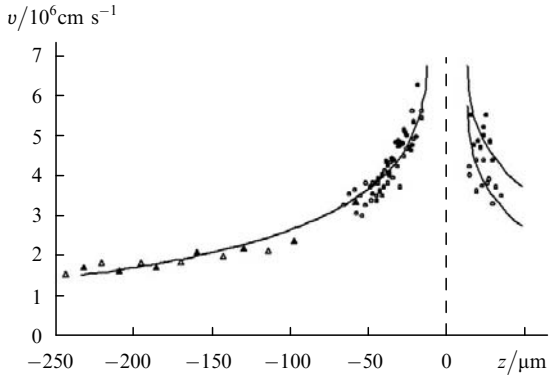

Figure 5. Velocities of the NLIS propagation to the focusing lens ($z < 0$) and in opposite direction measured by using beatings of adjacent (triangles) and well separated (circles) modes of laser radiation. Filled and open points correspond to different sets of experimental data.

(2) the maximum intensity of laser radiation scattered by a NLIS is observed near the beam waist, although the plasma front velocity here is close to maximal;

(3) the transverse size of a scattering track is smaller than 5 μm for the total length ~ 500 μm;

(4) the spatial modulation of radiation intensity scattered by a plasma reflects temporal variations in the laser pulse intensity (near the beam waist up to the beat period $\sim 90-100$ ps);

5) the scattering intensity is $\sim 10^2$ times higher for vertically-polarised laser radiation than for horizontally-polarised radiation;

(6) the h-component of scattered depolarised radiation for the vertically-polarised laser beam is very weak and has the spatial structure similar to that of the v-component;

(7) the intensity of the v-component of scattered depolarised radiation for the horizontally-polarised laser beam is close to that of the h-component but the v-component has a different structure consisting of two parallel tracks;

(8) the initiation of a NLIS can be delayed with respect to the laser intensity maximum by the time comparable with the pulse duration;

(9) the length of a scattering track weakly depends on the degree of excess over the breakdown threshold.

Consider possible reasons for the observed properties of laser radiation scattered by the NLIS plasma taking into account parameters of our experimental scheme. It was found in [11, 12] that radiation reflected from the plasma–undisturbed gas interface was detected in a similar scheme. This radiation enters the aperture of a microscope objective only if the plasma front surface has a certain shape. The most probable (and simple for consideration) due to the axial symmetry of the beam and the focusing system is a surface close to hemispherical. Its radius was estimated earlier as 2 μm [24]. Such a small radius, however, is not mandatory.

Consider the scheme in Fig. 6a, where the plasma front is represented by a spherical surface of radius r and the imaging microscope objective M with the focal distance f has diameter d, and analyse the conditions under which the laser beam propagating at an angle of γ to the axis of the focusing lens L can enter the objective aperture. It is easy to show that the laser beam enters the aperture of the microscope objective if

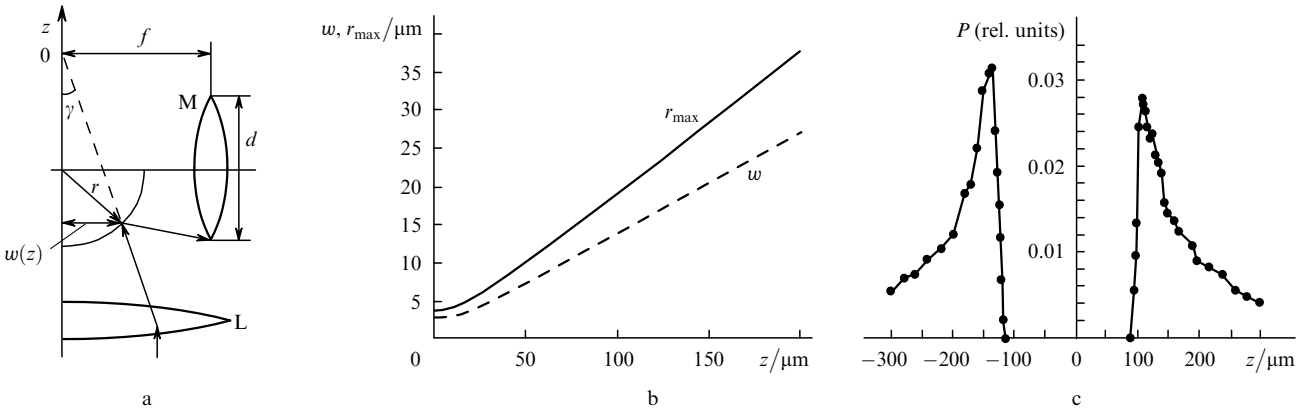

Figure 6. Scheme to the evaluation of the plasma front radius r_{max} (a), its values together with respective radii of the Gaussian beam (b), and the fraction of laser energy entring the aperture of the microscope objective with NA = 0.2 for the reflection from the spherical surface of $r = 20$ μm ($R = 100$ %) (c) versus the distance to the beam waist (M – microscope objective, L – lens).

$$r < r_{max} = w(z)\left[\cos\left(\frac{\pi}{4} - \frac{\gamma}{2} + \frac{1}{2}\arctan\frac{d}{2f}\right)\right]^{-1}, \qquad (1)$$

where

$$\gamma = \frac{dw(z)}{dz} = \frac{w_0}{z_R\left(1 + z_R^2/z^2\right)^{1/2}}$$

[far from the beam waist, $\gamma \approx \lambda/(\pi w_0)$]; the current radius $w(z)$ corresponds to a beam with the radius w_0 in the focal plane (at the e^{-2} beam intensity level); $z_R = \pi w_0^2/\lambda$ and $z = 0$ coresponds to the lens focus. Dependence (1) is shown in Fig. 6b for the microscope objective with NA = 0.2 and a Gaussian beam focused to a spot of radius $w_0 = 2$ μm. Far from the beam waist (for $z \gg z_R$), the relation $r < 1.37w(z)$ is fulfilled.

By using geometrical optics approximations for $z \gg z_R$, we shall see that if (1) is satisfied, then for a fixed value $|z|$ the radiation power entering the microscope objective is independent of the plasma front position with respect to the focal plane of the focusing lens L (although it decreases somewhat for $z > 0$ when plasma is behind the focal plane). Figure 6c shows that the dependence of the fraction P of the radiation energy entering the objective on z constructed for 4×10^4 rays randomly distributed over the 2-mm aperture ($F = 8$ mm). The radius curvature of the plasma front is set equal to 20 μm, which corresponds to the critical radius for $z = 100$ μm (Fig. 6b). This dependence is similar for reflection from the concave surface of the plasma front (in this case, the greater maximum is located at $z > 0$). The increase in $|z|$, and, hence, the decrease in the power density, should result in a rapid ($\sim 1/z^2$) decrease in the radiation intensity scattered from the plasma front. At the same time the change in the plasma front velocity with increasing $|z|$ upon time-integrated detection of scattering has the opposite tendency, which probably allows the observation of a plasma channel formed at the length exceeding the waist length ($2z_R$) by an order of magnitude.

Thus, calculations in the geometrical optics approximation correspond to the dependence in Fig. 6b obtained for a Gaussian beam and are in qualitative agreement with experimental results mentioned above in clauses (2) and (3). By using Fig. 6b, we can estimate the radius of curvature of the plasma front at the beginning of the scattering track as $r \approx 6 - 7$ μm. Of course, this radius can increase with distance from the beam waist, not exceeding its maximum value according to Eqn (1). The absence of noticeable scattering from the beam waist region can be explained by three reasons: the radius r does not satisfy relation (1), the velocity of the plasma front is extremely high, and the formation of the spark has the volume rather than the dot character. This also concerns the cases of the TEM_{01} and TEM_{02} modes (Figs 2b, c) for which, according to experimental data (Figs 2b–d), the existence of two independent plasma channels similar to that for the TEM_{00} mode can be assumed.

To explain a small traverse size of the scattering track in our model (clause 3) in the case of the detection scheme in Fig. 1, it is necessary to trace the trajectory of each of the beams directed to the focus of the lens L. The results of this calculation for the optical scheme with the above specified parameters are presented in Fig. 7. The left-hand column shows the lens aperture, the middle column demonstrates the plasma front surface observed from the aperture of the microscope objective, and the right-hand column illustrates the aperture of the microscope objective. Figure 7 shows only the beams satisfying condition (1). Figures 7a–c correspond to the displacement of the centre of curvature of the plasma front from the focal plane of the lens by 120 μm, and Figs 7d–f to the displacement by 100 μm.

Note that the scattering spot on the plasma front surface is much less than the radius of curvature of the front (the maximum size of the spot along the y axis is only 6 μm in Figs 7b, e). It seems that for this reason the recorded transverse size of the plasma channel is always small enough (at the limit of the optical resolution). It may seem that by changing the focusing of a microscope objective, it is possible to image on an array sensor (or a photographic film) the laser beam focused by a spherical of plasma surface, whose size, taking into account a small radius of curvature of the reflecting 'mirror', should be much smaller than the spot size in Figs 7b, e. However, it is impossible because of diffraction limitations. The aperture of the marked part of the laser beam is very small [on the lens it is 0.3 mm (Fig. 7a)], on the plasma front it is only 6 μm (Fig. 7b), which is equivalent to a substantial increase in the beam waist radius formed by the focusing lens and 'mirror' of radius r. The diffraction calculation by using the FRESNEL program [25] gives in this case the maximal diameter of the spot that is 2.4 times smaller than the spot

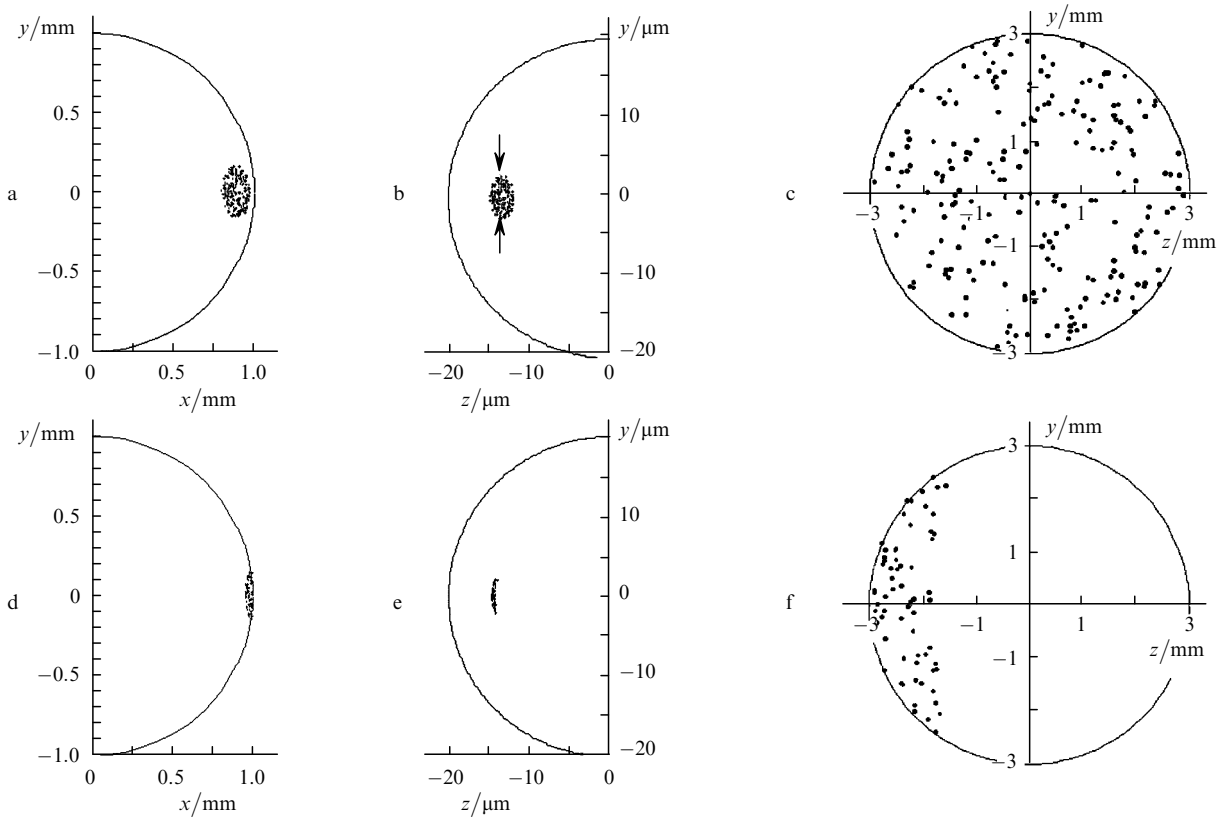

Figure 7. Results of beam tracing according to the scheme in Fig. 6a. Rays are shown on the focusing lens aperture (a, d), on the plasma front surface (b, e), and on the aperture of the microscope objective (c, f) for $z = 120$ μm (a–c) and 100 μm (d–f).

diameter on the plasma surface. The consideration of aberrations arising upon reflection from the spherical plasma front (the angle of incidence was $\sim 40^\circ$ for calculation parameters used) can only reduce this ratio. Thus, the minimal size of the scattering spot corresponds to the focusing of the optical system on the plasma front surface and is related only to the part of the plasma surface reflecting laser radiation into the microscope objective aperture.

The high-frequency spatial intensity modulation of radiation scattered by plasma near the beam waist has a period of $\sim 5 - 5.5$ μm, which is close to the transverse size of the scattering track. This parameter partly characterises the plasma front thickness responsible for the laser radiation reflection. This confirms the measurements of spatiotemporal streaks of spark images [11, 17, 24, 26].

Figure 2b also shows that behind the beam waist the scattering track can have a fracture which is associated, most likely, with the spatial variation in the structure of the laser beam propagating through the NLIS volume. The appearance of the diffractional maxima in this structure and transformation of the wavefront curvature during its propagation change conditions of reflection and/or the shape of the plasma front which can explain the revealed feature.

Thus, although the representation of the plasma boundary by a spherical surface is rather simplified, it demonstrated the general trend taking place upon the detection of the plasma channel by reflected laser radiation. The correctness of this approach is confirmed by analysis of polarisation measurements. For this purpose, calculations were performed for the same parameters of detecting optics and the plasma front (the electron density was $n_e = 10^{20}$ cm^{-3}). Only the beams reflected from the spherical plasma front laying on the line indicated by arrows in Fig. 7b were taken into account. The calculation results are presented in Fig. 8. Due to the difference in the reflection coefficients for V- and H-polarisations, the calculated ratio on the beam axis ($y = 0$) is $I_v(0)/I_h(0) = 115$ (the experimental value is $\sim 80 - 100$). This value weakly depends on the electron density and decreases to ~ 70 for $n_e = 10^{18}$ cm^{-3}.

For $y \neq 0$, when the electric vector is not in the plane drawn through the laser beam and the microscope objective axes (H-polarisation), or it is not perpendicular to it (V-polarisation) radiation is depolarised. In both cases this is manifested in the appearance of two maxima of the depolarised components which are symmetric with respect to the beam axis (dashed curves in Figs 8a, b). For the vertically-polarised initial laser beam, the calculated intensity ratio I_v/I_h is $\sim 4 \times 10^4$, while for the horizontally-polarised beam this ratio is $I_h/I_v \approx 3$. This is explained by a very small reflection coefficient for horizontally-polarised laser radiation compared to vertically-polarised radiation. Polarisation orientations of the initial beam and analyser cannot perfectly coincide, and the slightest deviations in their relative orientation considerably change the results of measurements. Thus, when the analyser orientation deviates by 1° the intensity distributions of the v and h depolarised components for vertically-polarised radiation are similar and the ratio I_v/I_h decreases to $\sim 3 \times 10^3$ (Fig. 8c). The ratio I_h/I_v for horizontally-polaried radiation almost does not vary (Fig. 8d) and only the asymmetry of the depolarised v-component appears. The inaccuracy of orientation of the initial beam polarisation of about 1° with respect to

the plane determined by the beam axis and the axis of the imaging optical system leads to the asymmetry of depolarised components. The change in the shape of the depolarised h-component for vertically-polarised laser radiation (the presence of one maximum instead of two) (Fig. 8c) is mainly determined by the inaccuracy of the orientation of the analyser with respect to this plane.

Thus, the model of spherical plasma front of the NLIS explains results of polarisation measurements of the scattered radiation (clauses 5–7) both qualitatively and quantitatively.

Finally, it is not excluded that the delay in the initiation of a NLIS, which in our case achieves 50 ns, appears only when short-focus lenses are used with the beam waist radius in focal plane of several microns and long (120 ns) laser pulse durations when the diffusion of electrons becomes considerable. The analysis of the NLIS initiation mechanisms (of the first stage of the spark dynamics) and the problem to which extent laser radiation affects the velocity of the plasma front expansion are outside the scope of this paper. However, we can assume that a weak dependence of the scattering track length corresponding to the position of the plasma front in time, on the laser pulse energy, and the absence of any substantial difference in the spark dynamics initiated on trailing edge of the pulse (followed by a decrease in the laser beam intensity) or on its leading edge (followed by an increase in the laser beam intensity) suggest the weak influence of laser radiation during the second stage of the NLIS evolution. Probably, this reflects only the specific character of the accomplished experiments. The influence of the laser pulse shape and its duration on the dynamics of the second stage of the NLIS evolution can be evaluated more accurately from the measurements of the spark expansion velocity based not only on accidental intensity modulations due to mode beatings.

4. Conclusions

In this work, we repeated the experiments that had been performed earlier during the time of intense interest in the NLISs. The use of laser radiation in the TEM_{00}, TEM_{01} and TEM_{02} modes for the spark initiation and modern detection techniques have allowed us to reveal a number of new features of the laser radiation scattered by the spark. The most interesting of them are the accurate localisation of the NLIS with respect to the laser beam waist, the low

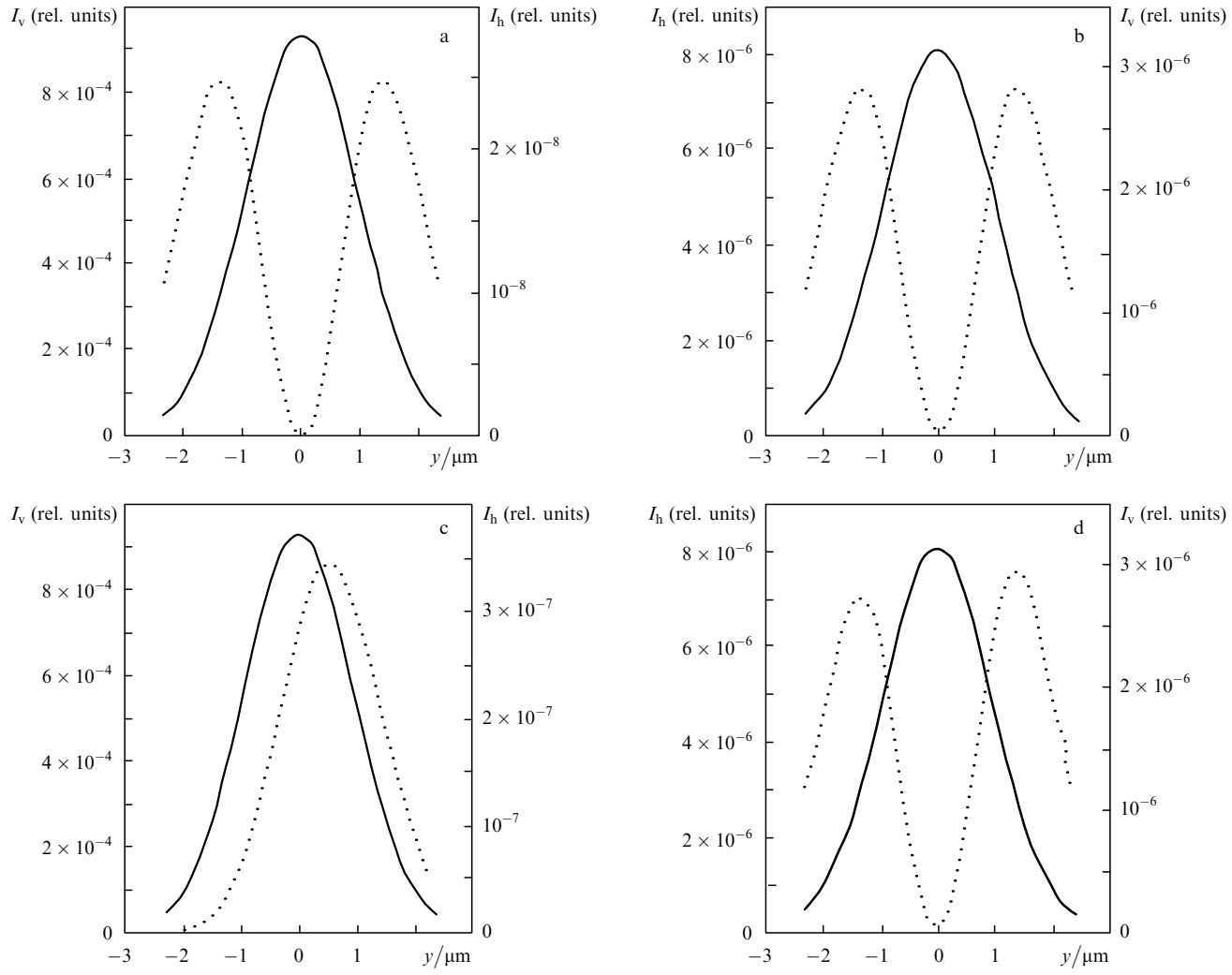

Figure 8. Intensity distributions of a V- (a, c) and H-polarised (b, d) laser beam reflected by the spherical plasma front in the case of ideal orientations of analyser and initial beam polarisation (a, b), and for the analyser turned off by 1° (c, d). Solid curves correspond to radiation with the initial polarisation, dotted curves correspond to the depolarised components.

level of scattering in this region, and the specific character of the depolarisation of scattered radiation. These and other characteristic properties, including those revealed earlier, can be described well enough within the framework of a simple model based on the nature of radiation scattering by the spark – the reflection from the plasma – undisturbed gas interface [11].

The representation of the plasma boundary by a spherical surface and consideration of the parameters of the optical scheme used for recording scattered radiation in the lateral direction allowed us to explain the experimental results, in particular, the scattering intensity ratio for V- and H-polarised laser radiation and their depolarisation. The absence of the quantitative agreement between calculations and measurements can be explained by several reasons, in particular, by the simplicity of our model and by the lack of data on the real electron density, its distribution on the plasma front, and dynamics of its variation.

Note also that we have observed the delay of the NLIS initiation with respect to the laser pulse maximum.

Acknowledgements. The author thanks V.Kh. Bagdasarov, S.V. Garnov, and N.N. Denisov for their help and assistance during experiments, and Yu.V. Senatsky and R.V. Serov for useful comments. This work was supported by the Russian Foundation for Basic Research (Grant No. 05-02-16818) and Grant No. NS-8283.2006.2 of the President of the Russian Federation for the state support of leading scientific schools.

References

1. Maker P.D., Terhune R.W., Savage C.M. *Quantum Electronics III*. Ed. by P. Grivet, N. Bloembergen (New York: Columbia University Press, 1964) p. 1559.
2. Ostrovskaya G.V., Zaidel' A.N. *Usp. Fiz. Nauk*, **111** (4), 579 (1973).
3. Morgan C.G. *Rep. Prog. Phys.*, **38**, 621 (1975).
4. Raizer Yu.P. *Usp. Fiz. Nauk.*, **87**, 29 (1965).
5. Longenecker M., Hüwel L., Cadwell L., Nassif D. *Appl. Opt.*, **42** (6), 990 (2003).
6. Yalĉin S., Crosley D.R., Smith G.P., Faris G.W. *Appl. Phys. B*, **68**, 121 (1999).
7. Basov N.G., Boiko V.A., Krokhin O.N., Sklizkov G.V. *Dokl. Akad. Nauk SSSR*, **173**, 538 (1967).
8. Alcock A.J., in *Laser Interaction and Related Plasma Phenomena*. Ed. by H.J. Schwarz, H. Hora (New York: Plenum Press, 1972) V. 2, p. 155.
9. Soubacq S., Pignolet P., Schall E., Baina J. *J. Phys. D: Appl. Phys.*, **37**, 2686 (2004).
10. Volkov V.A., Grigor'ev F.V., Kalinovskii V.V., et al. *Zh. Eksp. Teor. Fiz.*, **69**, 115 (1975).
11. Tomlinson R.G. *IEEE J. Quantum Electron.*, **5** (12), 591 (1969).
12. Savchenko M.M., Stepanov V.K. *Pis'ma Zh. Eksp. Teor. Fiz.*, **10**, 458 (1968).
13. Richardson M.C., Alcock A.J. *Appl. Phys. Lett.*, **18** (8), 357 (1971).
14. Askar'yan G.A. *Pis'ma Zh. Eksp. Teor. Fiz.*, **4**, 400 (1966).
15. Key M.H. *J. Phys. B*, **2**, 544 (1969).
16. Korobkin V.V., Motylev S.L. *Pis'ma Zh. Eksp. Teor. Fiz.*, **27** (10), 557 (1978).
17. Korobkin V.V., Alcock A.J. *Phys. Rev. Lett.*, **21**, 1433 (1968).
18. Wang Ch.C., Davis L.I. *Phys. Rev. Lett.*, **26** (14), 822 (1971).
19. Borghese A., Merola S.S. *Appl. Opt.*, **37**, 3977 (1998).
20. Dors I.G., Parigger C.G. *Appl. Opt.*, **42**, 5978 (2003).
21. Beduneau J.-L., Ikeda Y. *J. Quant. Spectr. Rad. Transfer*, **84**, 123 (2004).
22. Malyutin A.A., Ilyukhin V.A. *Kvantovaya Elektron.*, **37**, 181 (2007) [*Quantum Electron.*, **37**, 181 (2007)].
23. Catalogue of ThorLabs Inc. (Newton, NJ, USA, 2004) p. 273.
24. Ahmad N., Gale B.C., Key M.H. *J. Phys. B*, **2**, 403 (1969).
25. www.wavesimsoft.com.
26. Daiber J.W., Thompson H.M. *Phys. Fluids*, **10**, 1162 (1967).